



HAL
open science

Long-runout pyroclastic density currents: Analysis and implications

Olivier Roche, Christopher Henry, Nourddine Azzaoui, Arnaud Guillin

► **To cite this version:**

Olivier Roche, Christopher Henry, Nourddine Azzaoui, Arnaud Guillin. Long-runout pyroclastic density currents: Analysis and implications. *Geology*, 2022, 50 (10), pp.1172-1176. 10.1130/G50215.1 . hal-03792847

HAL Id: hal-03792847

<https://uca.hal.science/hal-03792847>

Submitted on 30 Sep 2022

HAL is a multi-disciplinary open access archive for the deposit and dissemination of scientific research documents, whether they are published or not. The documents may come from teaching and research institutions in France or abroad, or from public or private research centers.

L'archive ouverte pluridisciplinaire **HAL**, est destinée au dépôt et à la diffusion de documents scientifiques de niveau recherche, publiés ou non, émanant des établissements d'enseignement et de recherche français ou étrangers, des laboratoires publics ou privés.

1 Long-runout pyroclastic density currents: analysis and implications

2
3 Olivier Roche^{1*}, Christopher D. Henry², Nourddine Azzaoui³ and Arnaud Guillin³

4
5 ¹ *Laboratoire Magmas et Volcans, University Clermont Auvergne, CNRS, IRD, OPGC, 63000 Clermont-Ferrand,*
6 *France.*

7 ² *Nevada Bureau of Mines and Geology, University of Nevada, Reno, Nevada 89557, USA.*

8 ³ *Laboratoire de Mathématiques Blaise Pascal, University Clermont Auvergne, CNRS, 63000 Clermont-Ferrand,*
9 *France.*

10 * corresponding author (olivier.roche@uca.fr)

11 12 13 ABSTRACT

14
15 Pyroclastic density currents are hazardous, ground-hugging hot mixtures of gas and solid particles
16 produced by volcanoes. Currents generated by the largest explosive eruptions have traveled distances
17 on the order of 100 km, and their devastating impact has repeatedly marked Earth's geologic history.
18 We show that pyroclastic density currents from super-eruptions during the Oligocene in the Great Basin
19 of the United States had exceptional runout distances that may have exceeded 300 km. We present a
20 quantitative analysis of the data from these currents and consider, in particular, the areal extent of their
21 deposits (ignimbrites) as well as the relationship between their runout and the eruption mass discharge
22 rate. The ignimbrites have elliptical distributions characterized by axis length ratios of ~2-6, in contrast
23 to common subcircular ignimbrites, while the maximum runouts versus the discharge rates are clearly
24 outside the prediction intervals defined by other eruption data. We argue that the long runouts resulted
25 from the channeling of concentrated currents in regional paleovalleys whose gentle slope worked to
26 lengthen the travel distance. Our study demonstrates that these additional factors should be considered
27 in assessing hazards posed by future super-eruptions.

28 29 30 INTRODUCTION

31
32 Pyroclastic density currents (PDCs) that propagate over distances on the order of 100 km are
33 generated by the most powerful explosive volcanic eruptions (Wilson et al., 1995; Streck and Grunder,
34 1995; Kaneko et al., 2007; Best et al., 2013; Henry and John, 2013; Roche et al., 2016; Cisneros de León
35 et al., 2021). These gravity-driven hot mixtures of gas and solid particles are major natural hazards
36 because of the large areas they devastate, the amounts of ash they disperse into the atmosphere, and their
37 environmental consequences (Self, 2006). The particle transport mechanisms, which operate according
38 to the solid concentration (ϕ) increasing downwards and varying over several orders of magnitude, lead
39 to two types of PDCs (Lube et al., 2020): (1) dilute currents ($\phi < \sim 1$ vol. %) in which the turbulent gas
40 transports particles except in a basal bedload (Andrews and Manga, 2012; Brosch and Lube, 2020;
41 Dellino et al., 2021), and (2) two-layer currents (Shimizu et al., 2019) consisting of a concentrated basal
42 flow ($\phi > \sim 30$ vol.%) with dynamics controlled by particle interactions and gas pore pressure, which can
43 be fed by a dilute turbulent upper part through settling clusters of intermediate concentrations (Breard
44 et al., 2016). Recent advances suggest that this dichotomy may originate in the collapse dynamics of
45 eruptive fountains (Valentine, 2020). We refer to these two types of currents as “dilute” and
46 “concentrated” PDCs herein.

47 Earlier studies showed that the eruption mass discharge rate (MDR) is the fundamental parameter
48 controlling the runout of PDCs (Dade and Huppert, 1995; Bursik and Woods, 1996; Esposti Ongaro et
49 al., 2008; Roche et al., 2021) while increasing total volume of material expelled (positively correlated
50 with MDR; Roche et al., 2021) causes thicker deposits. PDCs with runout distances > 100 km are
51 generated by eruptions with the highest known eruptive rates ($\sim 10^{10}$ - 10^{11} kg/s) and are mostly associated
52 with caldera formation (Giordano and Cas, 2021). Other parameters such as particle settling velocity
53 and topography also control the runout of dilute and concentrated PDCs, respectively.

54 We investigated long-runout PDCs by analyzing the runout as a function of the MDR, using the
55 database and following the approach of Roche et al. (2021). We focused our analysis on concentrated

PDCs, including those that formed the ignimbrite flareup of the Great Basin (Best et al., 2013; Henry and John, 2013) for which we present new runout estimates, including one estimate >300 km. Herein, we use simplified names (e.g., Pahrnagat) to designate ignimbrites and parent PDCs.

GREAT BASIN IGNIMBRITES

Oligocene (23.0-31.7 Ma) ignimbrites of the Great Basin are predominantly rhyolites (Best et al., 2013; Henry and John, 2013). Source calderas were on a high (≥ 3 km) plateau (Cassel et al., 2012) with a north-south paleodivide in east-central Nevada, USA (Fig. 1A). The parent PDCs mostly flowed in deep, wide (0.6-1 \times 8-10 km) paleovalleys (Fig. 1B), particularly down valley to the west, and commonly across the Great Basin – Sierra Nevada structural-topographic boundary, which did not exist at the time, to the Pacific Ocean, which was then in the Great Valley of California (Supplemental Material). Ignimbrite correlation, which is based on stratigraphy, phenocryst assemblage, composition, remnant magnetization, and especially precise $^{40}\text{Ar}/^{39}\text{Ar}$ dates, demonstrates that at least seven PDCs flowed more than 200 km from their source, and the Pahrnagat flowed more than 300 km (Fig. 1; Table S1 in the Supplemental Material; all distances are corrected for post-emplacement extension). Almost all deposits are massive and densely to moderately welded even in the most distal outcrops, mostly lack associated stratified deposits, and – based on detailed and reconnaissance mapping – were confined to the deepest parts of paleovalleys, which indicates that they formed from concentrated flows (Fig. S1, Supplemental Material). Upper, poorly welded zones are rarely preserved because they were fluvially eroded in the paleovalleys from 0.1 Ma to >1.0 Ma between ignimbrite emplacement. Near their source, most PDCs spread short distances north or south perpendicular to major paleovalleys and entered only one or two west-draining paleovalleys. Two ignimbrites, Nine Hill and Campbell Creek (Fig. 1), spread considerably farther north and south and are found in as many as five major east-west paleovalleys in the Sierra Nevada. This may be because some tributaries are N-S oriented, valleys of any orientation were not deep near the paleodivide and source calderas – so avulsion of concentrated parts of the voluminous PDCs was possible – and/or some deposits could have been formed from dilute parts of the PDCs that crossed topographic barriers.

Aspect ratios (mean thickness over diameter of a circular deposit of equivalent area) of the Great Basin ignimbrites are close to, but higher than, the threshold value of $\sim 5 \times 10^{-5}$ given by Roche et al. (2021) and therefore indicate concentrated parent PDCs (Fig. 2), which is consistent with the sedimentological characteristics and deposit architecture. Note that the area of the Great Basin ignimbrites, which is delimited from peripheral outcrops, is overestimated due to confinement of the parent currents in regional paleovalleys. Hence, the aspect ratios we give are minimum estimates and the real values should be more in the field of concentrated PDCs.

A particularity of the Great Basin ignimbrites is their elliptical distribution around their respective source calderas (Fig. 3). We quantify this asymmetry using the ratio R_{max}/R of the maximum runout over the mean runout in sub-perpendicular directions (Fig. 3A). All ignimbrites (except Peach Spring) in the database of Roche et al. (2021) are characterized by $R_{\text{max}}/R < 1.5$, which we consider to be the upper threshold value for subcircular deposits. In contrast, the elliptical Great Basin ignimbrites have ratios significantly above this threshold (Fig. 3B). They are elongated in a broadly east-west direction that runs parallel to the regional valleys during PDC emplacement. The maximum runouts are always west of the calderas, consistent with the regional slope (Henry et al., 2012; their Fig. 8). However, in some cases (Campbell Creek, Nine Hill, Rattlesnake Canyon, and Underdown), PDCs also traveled long distances (~ 130 -200 km) eastward, probably because the calderas were close to the paleodivide and in the middle of the relatively flat plateau (Henry and John, 2013; Cassel et al., 2012). Some Great Basin ignimbrites have less elliptical distributions (i.e., R_{max}/R close to ~ 1.5) based on known outcrops. However, incomplete mapping in the east-central part of Fig. 1 limits interpretation (see the Supplemental Material).

ANALYSIS OF LONG RUNOUT DISTANCES

Fig. 4 shows the relationship between PDC runout, R , and mass discharge rate, Q . The cases with MDRs known from previous studies permit us to determine well-defined power law relationships (with coefficients of determination > 0.91) and prediction intervals that delineate the respective fields of

111 concentrated or dilute PDCs (Roche et al., 2021). Note that for concentrated PDCs, the relationship
112 $R=71\times 10^{-4}\times Q^{0.360}$ that we present is slightly different from that given by Roche et al. (2021; $R=55\times 10^{-4}\times Q^{0.373}$)
113 because Kidnappers (Wilson et al., 1995) and Rattlesnake ignimbrites (Streck and Grunder,
114 1995; not to be confused with Rattlesnake Canyon, which we present in this study) are ignored and we
115 define an average runout $R=81$ km (instead of 117 km) for Peach Spring due to the elliptical shape of
116 the ignimbrite (Roche et al., 2016; Supplemental Material).

117 For concentrated PDCs, the data for 40 subcircular ignimbrites for which we estimated the MDR
118 using a statistical fit to their bulk volumes (Supplemental Material) are all within the 99% prediction
119 intervals (Fig. 4A), which supports the hypothesis that the parent currents were concentrated. The mean
120 runouts of the elliptical Great Basin ignimbrites are also within these intervals except for those of Nine
121 Hill and Underdown, which are slightly outside. On the other hand, the R_{\max} values are clearly outside
122 the field of concentrated PDCs, and most currents are even outside that of dilute PDCs. This is also the
123 case for the subcircular Kidnappers and Rattlesnake ignimbrites whose shape, low aspect ratios and long
124 runouts are compatible with the emplacement of dilute PDCs. However, in both cases elongated
125 substrate masses in the ignimbrites (Wilson et al., 1995; Streck and Grunder, 1995) suggest erosion by
126 concentrated basal flows (cf. Roche et al., 2016). The broad welding of the Rattlesnake ignimbrite
127 further supports the emplacement of hot concentrated PDCs, at least in proximal and medial areas. In
128 this context, the most distal deposits could have been formed by the dilute upper part of the currents
129 traveling farther than the concentrated basal flow. To explain the long runout distance of ~ 185 km of
130 Kidnappers PDCs, Wilson et al. (1995) proposed that the currents travelled over a wet substrate of an
131 early phreatomagmatic fall material and boiled the water, which was a source of gas that fluidized the
132 (concentrated) basal flow. Note that MDRs inferred from bulk volumes may be underestimated;
133 however, the MDRs required for the R_{\max} data to be in the field of concentrated PDCs appear to be
134 unrealistic.

135 The Great Basin ignimbrites show that concentrated PDCs can travel distances of up to ~ 300 km
136 (i.e. Pahranaagat), approximately about three times farther than the maximum runouts reported for dilute
137 currents. Given our data, it appears that large, draining paleovalleys are a major cause of the exceptional
138 runouts of these PDCs. A lower MDR analog is the AD 1912 CE Katmai (Alaska, USA) eruption, during
139 which concentrated PDCs were confined to a valley (Fierstein and Hildreth, 1992). Interestingly, the
140 ~ 19 km runout at Katmai is close to the upper limit of concentrated PDCs at the same MDR of $\sim 10^9$ kg/s
141 (Fig. 4A), suggesting that runout enhancement was caused by flow confinement. Another key parameter
142 to explain the long runouts is the regional slope (Lindsay et al., 2001) although the correlation is not
143 systematic (Cas et al., 2011). In fact, recent simulations of dense, metric-scale gas-particle flows,
144 analogous to concentrated PDCs, show that the slope increases the runout distance by a factor of ~ 1.2
145 at 3° to ~ 2.2 at 10° relative to the horizontal (Aravena et al., 2021). As discussed by Aravena et al., this
146 runout increase would be even greater in nature because high gas pore pressure would be maintained for
147 longer durations than at a smaller length scale.

148 The data for the four dilute PDCs with volume-inferred MDR are within their corresponding field
149 (Fig. 4B). All of the data are also outside the field of the concentrated currents, except for that of the
150 Neapolitan Yellow Tuff lower member (Scarpati et al., 2015), for which a dilute, turbulent emplacement
151 is nonetheless supported by the deposit aspect ratio (Fig. 2) and by field evidence. The parent currents
152 of the Ata and Aso 4I-1 ignimbrites have runouts of 92 km and 88 km, respectively (Kaneko et al.,
153 2007), which are close to the maximum distance known for dilute PDCs (~ 125 km at Los Chocoyos;
154 Cisneros de León et al., 2021). The dilute nature of the Ata PDCs is supported by the presence of an
155 underlying ground-layer such as was described for the Taupo (New Zealand; Walker et al., 1981) and
156 Campanian (Italy; Scarpati et al., 2015) ignimbrites and which is thought to result from the efficient
157 segregation of coarse particles in the head and/or base of a turbulent current. The Aso 4I-1 ignimbrite
158 ($R=88$ km, $V_{\text{bulk}}=60$ km³, inferred MDR = 1.1×10^{10} kg/s) has characteristics similar to those of Taupo
159 (Wilson et al, 1985; 80 km, 30 km³, 5.3×10^{10} kg/s) but also has a welded valley-pond facies. The latter
160 suggests that the Aso 4I-1 PDCs may have emplaced as particular two-layer currents driven by a dilute
161 upper suspension as proposed by Roche et al. (2021) for Taupo (which has no welded facies), but with
162 more efficient heat retention and/or less effective entrainment of ambient air given the similar
163 temperatures of the respective magmas, i.e. 810-850°C for Aso 4I-1 (Kaneko et al., 2007) and 840-
164 860°C for Taupo (Smith et al., 2005).

165

166 CONCLUSION

167
168 Our study shows that dilute turbulent PDCs, whose propagation is generally independent of
169 topography and limited by buoyancy reversal due to entrainment and heating of the ambient air
170 (Andrews and Manga, 2012), have runouts that rarely exceed ~100 km. In contrast, concentrated PDCs
171 can travel much longer distances. This is primarily due to high MDRs of typically $>10^{10}$ kg/s and
172 sustained high gas pore pressure (Roche et al., 2016). Apart from specific conditions of flow
173 emplacement (cf. Kidnappers ignimbrite), the example of the Great Basin ignimbrites shows that
174 channelization of concentrated flows in regional valleys, even with gentle slopes, is an essential factor
175 in enhancing the runout distance. It must be also kept in mind that the dilute parts of two-layer PDCs
176 may impact even larger areas. The (minimum) runouts of up to ~300 km that we report show that the
177 PDCs generated during past super-eruptions are natural hazards with consequences are beyond any
178 human experience. However, these events are not that rare since the last super-eruptions occurred 7.3
179 k.y., 25.4 k.y., and 75 k.y. ago, respectively at Kikai (Japan), Oruanui (New Zealand) and Toba
180 (Indonesia); Miller and Wark (2008, p. 14) state: "the probability of a super-eruption in our lifetime is
181 not zero." Future super-eruptions at locations where the present-day combination of volcanic activity
182 and topography is similar to that of the Great Basin in the Oligocene would have dramatic consequences.
183 Likely sites include Yellowstone (USA), Campi Flegrei (Italy), Taupo volcanic zone (New-Zealand),
184 Laguna del Maule volcanic field (Andes), and Aso (Japan). Anticipating these extreme events with
185 appropriate simulation tools is an immense challenge for the scientific community (Esposti Ongaro et
186 al., 2020).

187 188 189 ACKNOWLEDGEMENTS

190
191 We thank Martin Streck for sharing unpublished data on the Rattlesnake tuff, and Yujiro Suzuki
192 and Benjamin Andrews for constructive reviews. This project is part of the French government IDEX-
193 ISITE initiative 16-IDEX-0001 (CAP 20-25). This is Laboratory of Excellence ClerVolc (Centre
194 Clermontois de Recherche sur le Volcanisme) contribution no. 539.

195
196
197 We present supplementary figures, detailed information on the Great Basin ignimbrites and the
198 paleovalleys, a summary of the database and the characteristics of the pyroclastic density currents, and
199 the statistical model we use.

200 201 202 REFERENCES CITED

- 203
204 Andrews, B., and Manga, M., 2012, Experimental study of turbulence, sedimentation, and coignimbrite mass partitioning in
205 dilute pyroclastic density currents: *Journal of Volcanology and Geothermal Research*, v. 225-226, p. 30-44, doi:
206 10.1016/j.jvolgeores.2012.1002.1011.
- 207 Aravena, A., Chupin, L., Dubois, T. and Roche, O., 2021, The influence of gas pore pressure in dense granular flows: numerical
208 simulations versus experiments and implications for pyroclastic density currents. *Bulletin of Volcanology*, v. 83, 77, doi:
209 <https://doi.org/10.1007/s00445-021-01507-7>.
- 210 Best, M.G., Christiansen, E.H., Deino, A.L., Gromme, S., Hart, G.L., and Tingey, D.G., 2013, The 36–18 Ma Indian Peak–
211 Caliente ignimbrite field and calderas, southeastern Great Basin, USA: Multicyclic super-eruptions: *Geosphere*, v. 9, no.
212 4, p. 964-950, doi: 910.1130/GES00902.00901.
- 213 Breard, E.C.P., Lube, G., Jones, J.R., Dufek, J., Cronin, S.J., Valentine, G.A., and Moebis, A., 2016, Coupling of turbulent and
214 non-turbulent flow regimes within pyroclastic density currents: *Nature Geoscience*, v. 9, p. 767-771, doi:
215 710.1038/NGEO2794.
- 216 Brosch, E. and Lube, G., 2020; Spatiotemporal sediment transport and deposition processes in experimental dilute pyroclastic
217 density currents: *Journal of Volcanology and Geothermal Research*, v. 401, 106946,
218 doi:<https://doi.org/10.1016/j.jvolgeores.2020.106946>.
- 219 Bursik, M.I., and Woods, A.W., 1996, The dynamics and thermodynamics of large ash-flows.: *Bulletin of Volcanology*, v. 58,
220 p. 175-193.
- 221 Cas, R.A.F., Wright, H.M.N., Folkes, C.B., Lesti, C., Porreca, M., Giordano, G., and Viramonte, J.G., 2011, The flow dynamics
222 of an extremely large volume pyroclastic flow, the 2.08-Ma Cerro Galán Ignimbrite, NW Argentina, and comparison with
223 other flow types: *Bulletin of Volcanology*, v. 73, p. 1583-1609, doi: 1510.1007/S00445-00011-00564-Y.
- 224 Cassel, E.J., Graham, S.A., Chamberlain, C.P. and Henry, C.D., 2012, Early Cenozoic topography, morphology, and tectonics

225 of the northern Sierra Nevada and western Basin and Range: *Geosphere*, v. 8, p. 229-249.

226 Cisneros de León, A., Schindlbeck-Belo, J. C., Kutterolf, S., Danisik, M., Schmitt, A. K., Freundt, A., Pérez, W., Harvey, J.

227 C., Wang, K.-L., and Lee, H.-Y., 2021, A history of violence: magma incubation, timing and tephra distribution of the Los

228 Chocoyos supereruption (Atitlán Caldera, Guatemala): *Journal of Quaternary Science*, v. 36, no. 2, p. 169-179,

229 doi:10.1002/jqs.3265.

230 Dade, W.B., and Huppert, H.E., 1995, A box model for non-entraining, suspension-driven gravity surges on horizontal surfaces:

231 *Sedimentology*, v. 42, p. 453-471.

232 Dellino, P., Dioguardi, F., Rinaldi, A., Sulpizio, R., and Mele, D., 2021, Inverting sediment bedforms for evaluating the hazard

233 of dilute pyroclastic density currents in the field: *Scientific Reports*, v. 11, p. 21024, [https://doi.org/10.1038/s41598-021-](https://doi.org/10.1038/s41598-021-00395-3)

234 [00395-3](https://doi.org/10.1038/s41598-021-00395-3).

235 Esposti Ongaro, T., Cerminara, M., Charbonnier, S.J., Lube, G., and Valentine, G.A., 2020, A framework for validation and

236 benchmarking of pyroclastic current models: *Bulletin of Volcanology*, v. 82, p. 51, [https://doi.org/10.1007/s00445-020-](https://doi.org/10.1007/s00445-020-01388-2)

237 [01388-2](https://doi.org/10.1007/s00445-020-01388-2).

238 Esposti Ongaro, T., Neri, A., Menconi, G., deMichieli Vitturi, M., Marianelli, P., Cavazzoni, C., Erbacci, G., and Baxter, P.J.,

239 2008, Transient 3D numerical simulations of column collapse and pyroclastic density current scenarios at Vesuvius: *Journal*

240 *of Volcanology and Geothermal Research*, v. 178, p. 378-396, doi:310.1016/j.jvolgeores.2008.1006.1036.

241 Fierstein, J., and Hildreth, W., 1992, The plinian eruptions of 1912 at Novarupta, Katmai National Park, Alaska: *Bulletin of*

242 *Volcanology*, v. 54, p. 646-684.

243 Giordano, G., and Cas, R.A.F., 2021, Classification of ignimbrites and their eruptions: *Earth Science Reviews*, v. 220, p.

244 103697, <https://doi.org/10.1016/j.earscirev.2021.103697>.

245 Henry, C.D., Faulds, J.E., dePolo, C.M. and Davis, D.A., 2004, Geology of the Dogskin Mountain Quadrangle, northern Walker

246 Lane, Nevada: Nevada Bureau of Mines and Geology Map 148, scale 1:24,000, 1 plate, 13 text pages.

247 Henry, C.D., Hinz, N. H., Faulds, J.E., Colgan, J.P., John, D.A., Brooks, E.R., Cassel, E.J., Garside, L.J., Davis, D.A., and

248 Castor, S.B., 2012, Eocene–Early Miocene paleotopography of the Sierra Nevada–Great Basin–Nevadaplano based on

249 widespread ash-flow tuffs and paleovalleys: *Geosphere*, v. 8, no. 1, p. 1-27, doi:10.1130/GES00727.00721.

250 Henry, C.D., and John, D.A., 2013, Magmatism, ash-flow tuffs, and calderas of the ignimbrite flareup in the western Nevada

251 volcanic field, Great Basin, USA: *Geosphere*, v. 9, no. 3, p. 951-1008, doi:10.1130/GES00867.00861.

252 Kaneko, K., Kamata, H., Koyaguchi, T., Yoshikawa, M., and Furukawa, K., 2007, Repeated large-scale eruptions from a single

253 compositionally stratified magma chamber: An example from Aso volcano, Southwest Japan: *Journal of Volcanology and*

254 *Geothermal Research*, v. 167, p. 160-180, doi:110.1016/j.jvolgeores.2007.1005.1002.

255 Lindsay, J.M., de Silva, S., Trumbull, R., Emmermann, R., and Wemmer, K., 2001, La Pacana caldera, N. Chile: a re-evaluation

256 of the stratigraphy and volcanology of one of the world's largest resurgent calderas: *Journal of Volcanology and Geothermal*

257 *Research*, v. 106, p. 145-173.

258 Lube, G., Breard, E.C.P., Esposti-Ongaro, T., Dufek, J., and Brand, B., 2020, Multiphase flow behaviour and hazard prediction

259 of pyroclastic density currents: *Nature Reviews Earth & Environment*, v. 1, p. 348-365, [https://doi.org/10.1038/s43017-](https://doi.org/10.1038/s43017-020-0064-8)

260 [020-0064-8](https://doi.org/10.1038/s43017-020-0064-8).

261 Miller, C.F., and Wark, D.A., 2008, Supervolcanoes and their explosive supereruptions: *Elements*, v. 4, p. 11-16,

262 doi:10.2113/GSELEMENTS.4.1.11

263 Roche, O., Azzaoui, N., and Guillin, A., 2021, Discharge rate of explosive volcanic eruption controls runout distance of

264 pyroclastic density currents: *Earth and Planetary Science Letters*, v. 568, p. 117017, doi:

265 <https://doi.org/10.1016/j.epsl.2021.117017>.

266 Roche, O., Buesch, D. C., and Valentine, G. A., 2016, Slow-moving and far-travelled dense pyroclastic flows during the Peach

267 Spring super-eruption: *Nature Communications*, v. 7, p. 10890, doi: 10810.11038/ncomms10890.

268 Scarpati, C., Sparice, D., and Perrotta, A., 2015, The ground layer of the Campanian Ignimbrite: an example of deposition from

269 a dilute pyroclastic density current: *Bulletin of Volcanology*, v. 77, p. 97, doi: 10.1007/s00445-00015-00985-00440.

270 Self, S., 2006, The effects and consequences of very large explosive volcanic eruptions: *Philosophical Transactions of the*

271 *Royal Society: A, Mathematical, Physical and Engineering Sciences*, v. 364, p. 2073–2097, doi:2010.1098/rsta.2006.1814.

272 Shimizu, H.A., Koyaguchi, T., and Suzuki, Y.J., 2019, The run-out distance of large-scale pyroclastic density currents: A two-

273 layer depth-averaged model: *Journal of Volcanology and Geothermal Research*, v. 381, p. 168-184,

274 <https://doi.org/110.1016/j.jvolgeores.2019.1003.1013>.

275 Smith, V. C., Shane, P., and Nairn, I.A., 2005, Trends in rhyolite geochemistry, mineralogy, and magma storage during the last

276 50 kyr at Okataina and Taupo volcanic centres, Taupo Volcanic Zone, New Zealand: *Journal of Volcanology and*

277 *Geothermal Research*, v. 148, p. 372-406, doi: 10.1016/j.jvolgeores.2005.05.005.

278 Streck, M.J., and Grunder, A.L., 1995, Crystallization and welding variations in a widespread ignimbrite sheet; the Rattlesnake

279 Tuff, eastern Oregon, USA: *Bulletin of Volcanology*, v. 57, p. 151-169.

280 Valentine, G.A., 2020, Initiation of dilute and concentrated pyroclastic currents from collapsing mixtures and origin of their

281 proximal deposits: *Bulletin of Volcanology*, v. 82, p. 20, <https://doi.org/10.1007/s00445-00020-01366-x>.

282 Walker, G.P.L., Self, S., and Frogatt, P.C., 1981, The ground layer of the Taupo ignimbrite: a striking example of sedimentation

283 from a pyroclastic flow: *Journal of Volcanology and Geothermal Research*, v. 10, p. 1-11.

284 Wilson, C.J.N., 1985, The Taupo eruption, New Zealand II. The Taupo ignimbrite: *Philosophical Transactions of the Royal*

285 *Society of London: A, Mathematical, Physical and Engineering Sciences*, v. 314, p. 229-310,

286 <https://doi.org/10.1098/rsta.1985.0020>.

287 Wilson, C.J.N., Houghton, B.F., Kamp, P.J.J., and McWilliams, M.O., 1995, An exceptionally widespread ignimbrite with

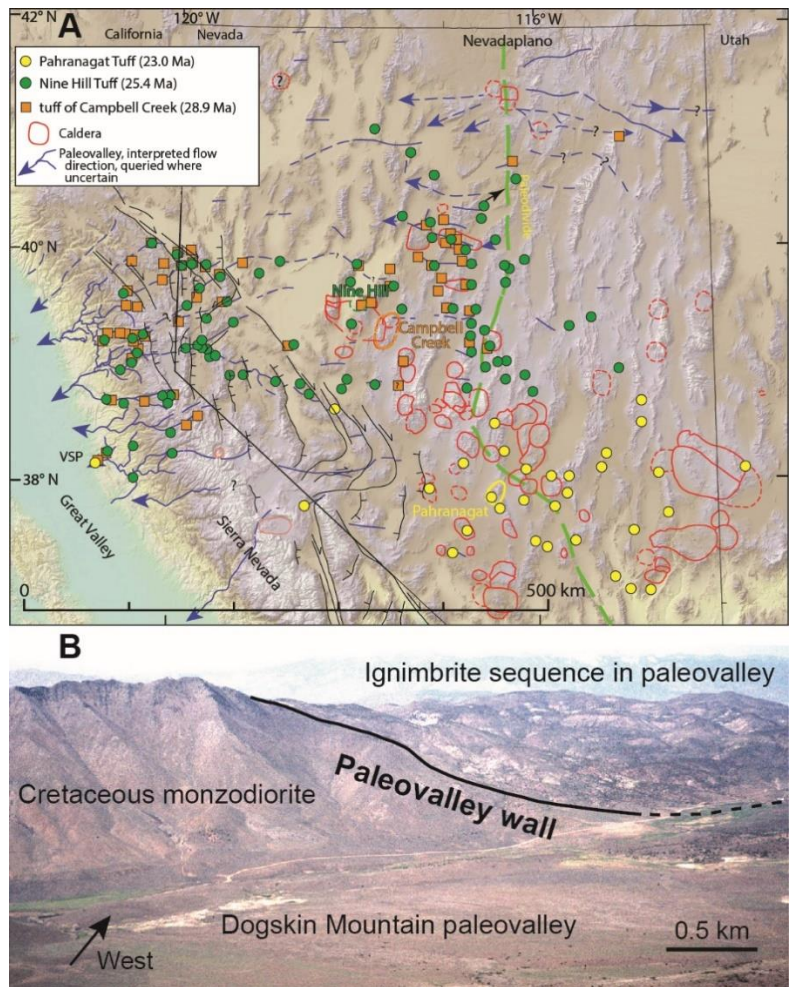
288 implications for pyroclastic flow emplacement: *Nature*, v. 378, p. 605-607.

289

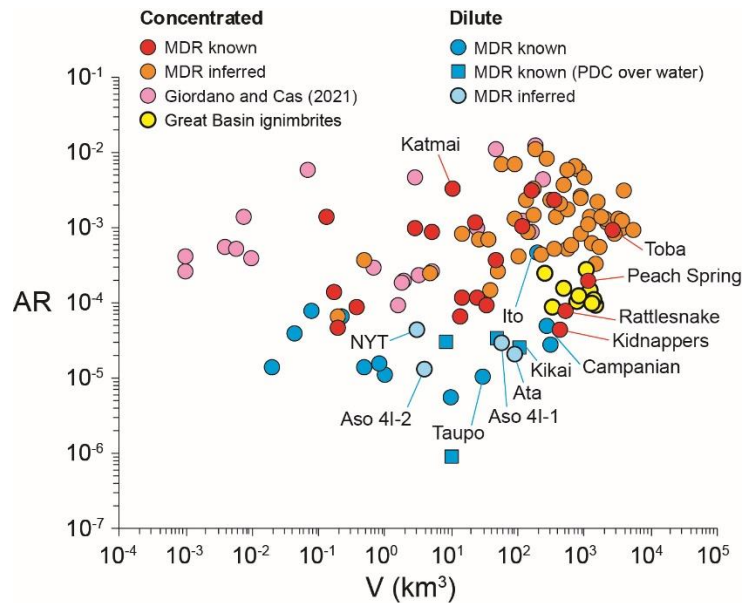
290

291

292 FIGURES
293
294

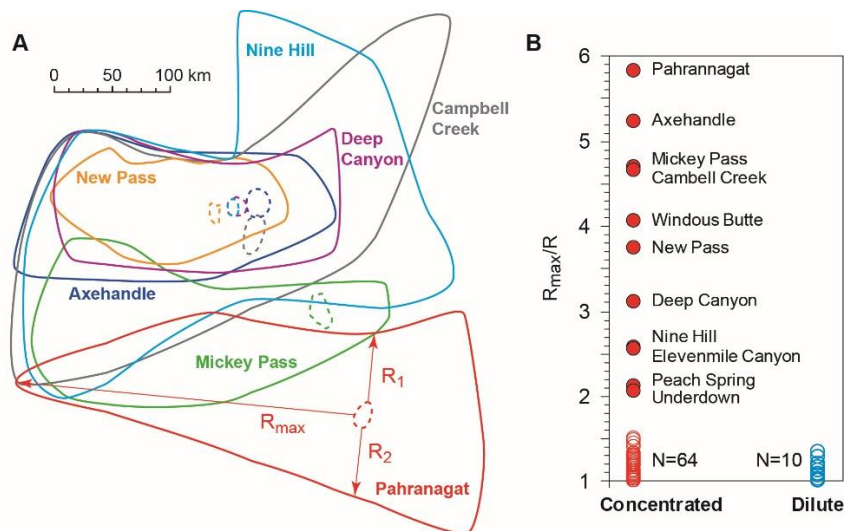


295
296
297 **Figure 1.** (A) Paleovalley systems and calderas of the Great Basin and Sierra Nevada (Henry and John,
298 2013; and references therein). Parent pyroclastic density currents of the 28.9 Ma Campbell Creek, 25.4
299 Ma Nine Hill and 23.0 Ma Pahranaagat ignimbrites flowed ~228 km, ~285 km and ~314 km, respectively,
300 westward from their source calderas (distances were corrected for post-emplacment extension, see
301 Supplemental Material). VSP: Valley Springs Peak. (B) Aerial view westward to paleovalley partly
302 filled with a sequence of 18 separate ignimbrites in western Nevada (Henry et al., 2004). Paleovalley is
303 ~0.7 km deep and >7 km wide (north end is faulted).
304
305



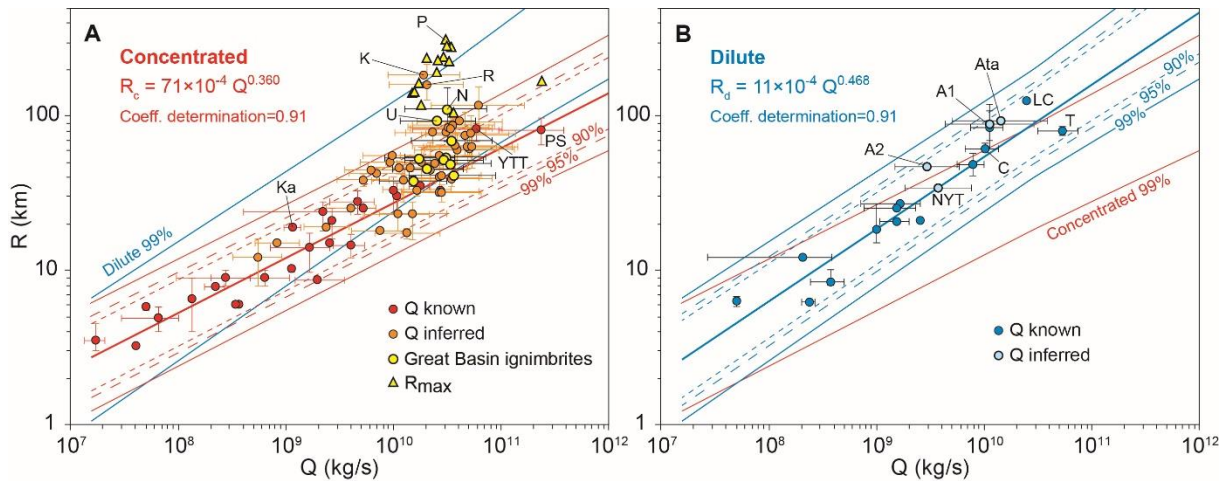
306
 307 **Figure 2.** Aspect-ratio (AR) as a function of bulk volume (V) of outflow ignimbrite. We distinguish the
 308 cases of parent-concentrated or dilute pyroclastic density currents (PDCs), for which the mass discharge
 309 rates (MDR) are known from earlier studies or inferred from our analysis (Supplemental Material; Table
 310 S2), are distinguished. The ignimbrites discussed in the main text are indicated (NYT: Neapolitan
 311 Yellow Tuff). The specific case of Ito was discussed by Roche et al. (2021).

312
 313



314
 315 **Figure 3.** (A) Simplified map view of some Great Basin ignimbrites (detailed maps are provided in the
 316 Supplementary Material). Relative latitudes are true and distances have been corrected for E-W
 317 extension. Dashed polygons represent the source calderas. (B) Ratio of the maximum runout, R_{max} , to
 318 the mean runout, $R=(R_1+R_2)/2$ as defined in panel A, for ignimbrites formed by concentrated or dilute
 319 pyroclastic density currents (N —number of ignimbrites, data from Roche et al., 2021; Supplemental
 320 Material; Table S2). The Great Basin and the Peach Spring ignimbrites are distinguished from
 321 subcircular ignimbrites by $R_{max}/R > 1.5$.

322



323
 324 **Figure 4.** pyroclastic density currents (PDC) runout, R , as a function of the mass discharge rate, Q , for
 325 (A) concentrated and (B) dilute PDCs. Power law relationships and prediction intervals of 90%, 95%
 326 and 99% are determined from eruptions for which the mass discharge rates are known (Roche et al.,
 327 2021). For the other eruptions, Q is inferred from ignimbrite bulk volume estimates, and 95% confidence
 328 error bars are given (Supplemental Material). For the Great Basin and Peach Spring ignimbrites, R is
 329 the mean runout in directions sub-perpendicular to those of the maximum runout R_{\max} . The cases
 330 discussed in the main text are indicated: (A) Ka: Katmai, K: Kidnappers, N: Nine Hill, P: Pahranagat,
 331 PS: Peach Spring, R: Rattlesnake (Streck and Grunder, 1995), U: Underdown, YTT: Young Toba tuff;
 332 (B) A1: Aso 4I-1, A2: Aso 4I-2, C: Campanian, LC: Los Chocoyos, NYT: Neapolitan Yellow tuff, T:
 333 Taupo.
 334